Bulgarian Chemical Communications, Volume 49, Special Edition B (pp. 176 – 182) 2017

Total oxidation of ethyl acetate on nanostructured manganese-cerium oxide catalysts supported on mesoporous silica

R. N. Ivanova*, T. S. Tsoncheva

Institute of Organic Chemistry with Centre of Phytochemistry, Bulgarian Academy of Sciences, 1113 Sofia, Bulgaria

Received February 21, 2017; Revised March 08, 2017

Dedicated to Acad. Bogdan Kurtev on the occasion of his 100th birth anniversary

Current investigation is focused on the texture effect of mesoporous silica support on the structure, redox and catalytic properties of hosted in it nanosize mono- and bi-component manganese-cerium oxides. Mesoporous silicas type SBA-15 and KIT-6 with uniform cylindrical mesopores, packed in 2D- and 3D-symmetry respectively, was used as a support. A complex of physicochemical techniques, such as nitrogen physisorption, X-ray diffraction, UV-Vis spectroscopy and temperature-programmed reduction with hydrogen were used for the samples characterization. The potential application of the composites as catalysts for ethyl acetate combustion was studied. It was demonstrated that SBA-15 and KIT-6 could be good host matrix for the stabilization of highly dispersed manganese-ceria oxide particles. Strong effect of mesoporous silica support topology, which also depends on the samples composition, on the formation of catalytic active sites was established.

Key words: manganese-cerium oxides; SBA-15 and KIT-6 mesoporous silica; ethyl acetate oxidation

INTRODUCTION

Volatile organic compounds (VOCs) are considered as one of the major pollutants emitted from the industrial processes, transport and human activity and most of them are identified as carcinogenic and teratogenic [1]. Nowadays, the increasing political, social and economic attention on the environment and the quality of life has enforced the strict monitoring of VOCs emission and the development of efficient technologies for their elimination. The catalytic total oxidation has been recognized as more economic process even when VOCs were emitted in low concentrations [2–7]. It works at relatively lower operation temperatures and with higher efficiency compared to thermal combustion techniques, avoiding the supplementary use of fuel and reducing air contamination due to NO_x formation [1, 8]. Despite noble metals are commonly used catalysts owing to their high catalytic activity, transition metal oxides could be also good alternative due to their low cost, accessibility and stability to different pollutants [1]. During the last decade the efforts have been directed to the increase in their catalytic activity by the miniaturization in nanoscale and mesoporous silicas were considered as a suitable host matrix for the preparation and stabilization of metal oxide nanoparticles. It was reported that ceria-based catalysts exhibit high activity in VOCs oxidation due to their unique high oxygen storage capacity associated with facile Ce^{4+}/Ce^{3+} redox transition [8, 9]. Manganese oxide materials are also known as efficient catalysts for various redox processes due to the multivalent state of Mn ions [1, 10]. Obviously, this provides good catalyst potential of Ce–Mn mixed oxides and their behaviour has already been tested in number of catalytic processes, such as complete oxidation of ethanol [3], formaldehyde, hexane [11], selective catalytic reduction (SCR) of NO with NH_3 [12] catalytic oxidation of diesel soot [13] *etc.* In this study, we focused our attention on the development of nanostructured Mn–Ce mixed oxides by their deposition on mesoporous silica support. The pore topology effect on the control of phase composition and catalytic behaviour of Mn–Ce oxides was studied using mesoporous silicas with almost uniform cylindrical pores arranged in 2D- (SBA-15) or 3D- (KIT-6) structure as a support. The catalytic activity of the obtained composites was tested in ethyl acetate combustion.

EXPERIMENTAL

Materials

SBA-15 and KIT-6 mesoporous silicas were prepared by hydrothermal synthesis at 373K using

* To whom all correspondence should be sent:
E-mail: *rivanova@orgchm.bas.bg*

Pluronic P123 triblock- co-polymer ($EO_{20}PO_{70}EO_{20}$) as structure-directing agent according to the procedures described in [14] and [15], respectively. The silica modification was carried out by incipient wetness impregnation technique using 1.2 M aqueous solution of $Mn(NO_3)_2.4H_2O$ and/or $Ce(NO_3)_2.6H_2O$. The impregnated samples were dried at room temperature for 24 h and then treated in air at 773K for 2 h for precursor decomposition. The metal content in all modifications was set to be 6 wt.%. The obtained materials were denoted as xMnyCe/S, where x/y represents the Mn/Ce ratio and S is the silica support used (SBA-15 or KIT-6).

Methods of characterization

The nitrogen physisorption data were obtained by nitrogen adsorption at 77 K on Quantachrome NOVA 1200 apparatus. S_{BET} was calculated applying the Brunauer, Emmet and Teller (BET) equation for N_2 relative pressure in range of 0.05\P/P0\0.30, and the pore size distribution was determined by the DFT method applied to the adsorption branch of the isotherm. The t-plot method was used for the estimation of micropores parameters. The powder X-ray diffraction spectra were recorded within the range from 1° to 80° 2Θ with on a Bruker D8 Advance diffractometer with Cu Ka radiation. The UV-Vis spectra were recorded on the powder samples using a Jasco V-650 UV-Vis spectrophotometer equipped with a diffuse reflectance unit. The TPR/TG (temperature-programmed reduction/thermo-gravimetric) analyses were performed on a Setaram TG92 instrument in a flow of 50 vol% H_2 in Ar (100 cm^3/min^{-1}) and heating rate of 5 K/min^{-1}. The catalytic experiments were performed in a flow type reactor (0.030 g of catalyst) with a mixture of ethyl acetate (1.21 mol%) in air with WHSV – 335 h^{-1}. Gas chromatographic (GC) analyses were carried out on HP5850 apparatus using carbon-based calibration. The samples were pretreated in Ar at 423K for 1 h and then the temperature was raised with a rate of 2K/min in the range of 423–773K.

RESULTS AND DISCUSSION

Nitrogen physisorption measurements were conducted in order to elucidate the textural properties of the studied samples. In Fig. 1 are presented nitrogen physisorption isotherms for both SBA-15 and KIT-6 silica supports and their mono- and bi-component Mn-Ce modifications. The texture parameters are listed in Table 1.

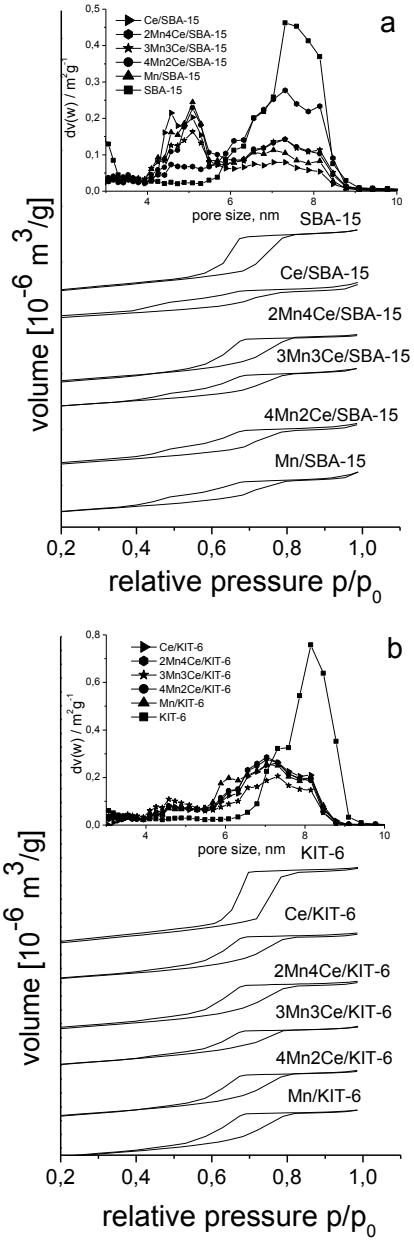

Fig. 1. Nitrogen physisorption isotherms with pore size distributions (inset) for the studied samples.

Nitrogen physisorption isotherms of SBA-15 and KIT-6 materials are of type IV with H1 hysteresis loop in the 0.4–0.8 P/P_0 region, which is typical of ordered mesoporous materials with uniform cylindrical mesopores. Note, that both supports possess almost similar BET surface area (800–850 m^2/g), total pore volume (1–1.2 cm^3/g) and average pore diameter of about 7–8 nm. The preservation of the isotherms after the modification indicates absence of structure collapse of the silica matrix.

Table 1. Texture characteristics of the obtained materials.

Sample	S_{BET}, m^2/g	V_{tot}, cm^3/g	V_{mic}, cm^3/g	V_{mes}, cm^3/g	$D_{av.p}$, nm
SBA-15	799	1.03	0.08	0.95	7.3
Ce/SBA-15	540	0.61	0.05	0.56	4.5
2Mn4Ce/SBA-15	629	0.79	0.05	0.74	5.0
3Mn3Ce/SBA-15	518	0.64	0.03	0.61	4.9
4Mn2Ce/SBA-15	575	0.68	0.03	0.65	4.7
Mn/SBA-15	528	0.67	0.03	0.64	5.1
KIT-6	872	1.23	0.14	1.09	8.2
Ce/KIT-6	664	0.79	0.04	0.75	7.3
2Mn4Ce/KIT-6	635	0.79	0.05	0.74	5.0
3Mn3Ce/KIT-6	593	0.68	0.04	0.64	4.6
4Mn2Ce/KIT-6	628	0.78	0.04	0.74	4.9
Mn/KIT-6	654	0.80	0.05	0.75	7.0

S_{BET} - specific surface area; V_{tot} - total pore volume; V_{mic} and V_{mes} - micro and mesopore volume, $D_{av.p}$ - average pore diameter

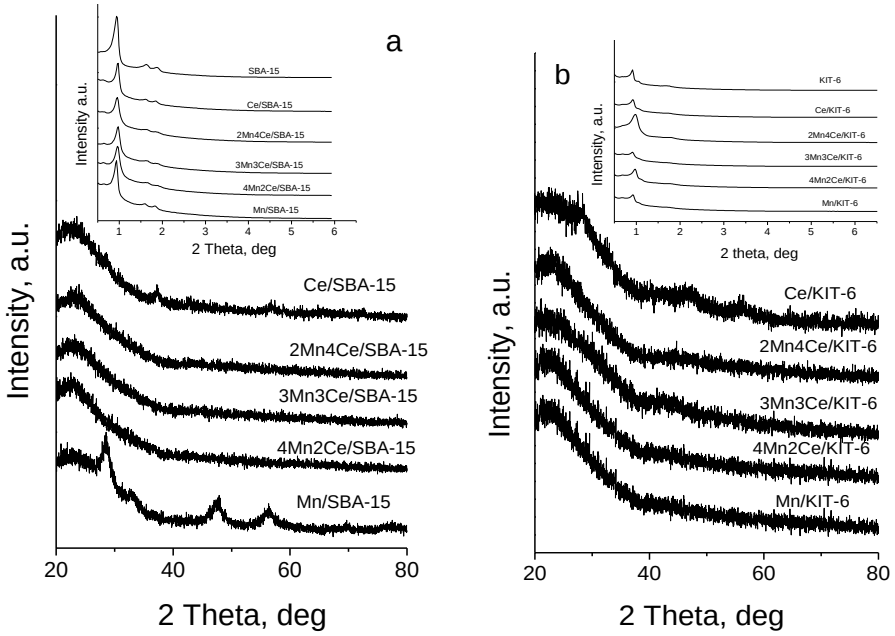

Fig. 2. XRD patterns of the studied samples in small (inset) and wide angle region.

The observed change in the shape of the desorption branch for all modifications as compared to the parent materials, which is more pronounced for the 2D- based ones, evidences pore blocking probably due to the deposition of metal oxide particles in them. This assumption was also confirmed with the observed decrease in the BET surface area and pore volume after the modification procedure (Table 1), again being more visible for the SBA-15 supported samples. The decrease in the maximum of pore size distribution peaks (Fig. 1 inset) combined with its shift to lower values clearly indicates location of manganese and ceria nanoparticles within the mesopore structure.

XRD patterns of parent and modified mesoporous materials are presented in Fig. 2.

In the small angle region (Fig. 2 inset), two diffraction peaks, indexed as (211) and (222) planes of cubic mesoporous structure, and three well resolved reflections, assigned to (100), (110) and (200) planes of hexagonally ordered mesopores, were registered for KIT-6 and SBA-15 materials, respectively [16]. These results indicate that the silica supports exhibit high quality ordered porous texture with 3D- and 2D-topology. After the impregnation, preservation of the ordered mesoporous structure was observed. The decrease in the intensities of the reflections could be due to a decrease in the electron density contrast upon introduction of metal oxide species into the silica host matrix. XRD pattern in the wide angle region of Ce/SBA-15 represents low intensive diffraction

peaks at 28.6^0, 33.0^0, 47.0^0 and 56.0^0 2θ, corresponding to highly dispersed CeO_2 particles (JCPDS 43-1002). In the case of Mn/SBA-15 the appearance of weak diffraction peaks at 28.6^0, $37^0.3$, 43.0^0 and 56.0^0 2θ could be assigned to highly dispersed α-MnO_2 (JCPDS 44-0141). The absence or the appearance of very broad reflections in the patterns of mixed manganese-ceria modifications indicates high dispersion of metal oxide phase on both silica supports, the effect being more pronounced for KIT-6.

UV-Vis analysis (Fig. 3) has been used to obtain information for the coordination and oxidative state of metal ions.

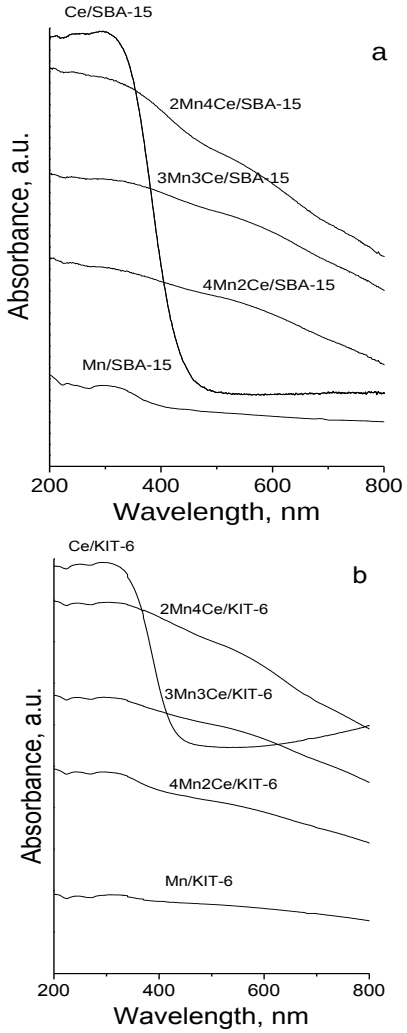

Fig. 3. UV-Vis spectra of SBA-15 and KIT-6 modifications.

The spectra of monocomponent ceria samples show well pronounced absorption peaks at about 265 and 300 nm, corresponding to charge transfer (CT) of O^{2-} to Ce^{3+} and O^{2-} to Ce^{4+}, respectively [17]. The absorption edge is significantly red-shifted for Ce/KIT-6 as compared to the Ce/SBA-15, which could be associated with the formation of more finely dispersed CeO_2 crystallites in the former material. Among the monocomponent manganese modifications, the observed absorption in the region 350–500 nm, could be due to the $O^{2-} \rightarrow Mn^{3+}$ CT transitions. The observed absorption at about 330 nm can be associated with the presence of Mn^{4+} ions in octahedral coordination [16] and this is in consistent with the XRD data. An increased absorption above 450 nm in the spectra of bi-component samples demonstrates changes in the environment and/or oxidation state of manganese ions.

Additional information for the redox properties of the studied materials was obtained by temperature-programmed reduction (TPR) with hydrogen (Fig. 4).

Data for the initial temperature of the reduction, the position of the maximum in DTG curves and the calculated reduction degree are presented in Table 2. The reduction of monocomponent ceria samples initiates above 650 K and the calculated reduction degrees for $Ce^{4+} \rightarrow Ce^{3+}$ transition [3] in the entire temperature region are 36 and 57% for Ce/SBA-15 and Ce/KIT-6, respectively. In accordance with data from XRD and UV-Vis analysis, the observed differences in the reduction degree can be attributed to the presence of more finely dispersed CeO_2 crystallites in the KIT-6 sample compared to its SBA-15 analogue. The TPR-DTG profiles of monocomponent Mn modifications show two reduction effects, which are generally assigned to step-wise reduction of MnO_2 or Mn_2O_3 to Mn_3O_4 and then to MnO [19, 20]. The reduction peaks of Mn/SBA-15 are narrower which could be associated to the presence of more uniform well crystallized particles and this is in consistence with the XRD data. The reduction degree for Mn/SBA-15 is lower than the expected theoretic one for the reduction of Mn^{4+}/ Mn^{3+} to Mn^{2+} (Table 2) which could be due to the: (1) predominant presence of manganese ions in lower oxidation state (Mn^{2+} and Mn^{3+}); (2) strong interaction of manganese species with the silanol groups of the support and/or (3) less accessibility of manganese species into the porous host matrix. The latter assumption is also confirmed by the nitrogen physisorption data (Table 1), where a significant decrease in the BET surface area is observed. For the 3D- based analogue, the experimental weight loss is higher than the calculated one for the Mn^{3+} to Mn^{2+} transition which indicates significant presence of Mn^{4+} ions. The reduction profiles for the binary materials are shifted to higher

temperatures in comparison with the corresponding pure Mn modifications, which reveal changes with the manganese phase. In case of SBA-15 binary samples the reduction degree preserves almost similar to that one for Mn/SBA-15. However significant decrease in the reduction degree occurs for all binary KIT-6 modifications. This could be due to the existence of strong interaction between the individual oxides which is controlled by the pore topology of silica support.

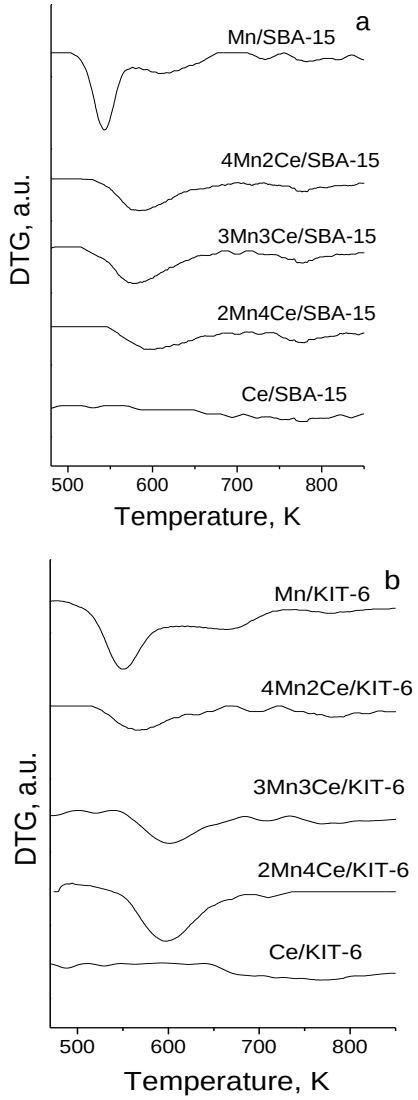

Fig. 4. TPR-DTG profiles of all manganese-ceria modifications.

The temperature dependencies of EA conversion within the range of 450–650 K are presented in Fig. 5a. All materials represent notable catalytic activity above 550 K and 80–100% conversion is achieved at 600–620 K. The main product of the conversion is CO_2, but ethanol (Et), acetaldehyde (AA) and acetic acid (AcAc) in different proportion are also registered as by-products. The changes in the selectivity in all investigated temperature interval are presented in Fig. 5b and the products distribution at 30% conversion is listed in Table 3. Among various modifications the highest catalytic activity combined with high selectivity to CO_2 is registered for Mn/KIT-6. Taking into account the physicochemical data, this could be assigned to higher dispersion of manganese oxide phase in 3D-silica support as compared to pure Mn/SBA-15.

Moreover, here domination of MnO_2 was assumed on the base of TPR and XRD data, which evidences the high activity of Mn^{4+}-Mn^{3+} redox pairs in total oxidation of EA. For comparison, the individual CeO_2 modified materials exhibit lower catalytic activity and high selectivity to ethanol formation. This could be understand taking into account that the EA oxidation typically proceeds as a step-wise process, starting with the hydrolysis to Et and AcAc and their further oxidation by Mars van Krevelen mechanism [21]. Obviously, the higher surface acidity of CeO_2 provokes the facile hydrolysis of EA. All binary materials possess lower catalytic activity than mono-component manganese ones but improved selectivity to CO_2 formation compared to ceria modifications. This could be provoked by the substitution of Mn^{4+} ions by Ce^{4+} and/ or increase in the number of Ce and Mn ions in lower oxidation state leading to the formation of oxygen vacancies. This ensures the activity of new type of active redox pairs and changes the acidic-base and redox properties of the solid. This assumption is confirmed by the significant changes in the UV-Vis spectra (Fig. 3) and the decrease in the reduction ability for the binary materials (Fig. 4), despite the improved dispersion as compared to the individual oxides (Fig. 2).

The more pronounced changes in the catalytic activity with the samples composition combined with higher selectivity to CO_2 for the KIT-6 based binary materials urge the authors to assume higher extent of interaction between the individual oxides in the more opened 3D-structure. The absence of simple relation between the catalytic activity of the samples and their composition (Table 3) evidences that pore topology of silica support controls not only the phase composition but also the accessibility of the active species for the reactant molecules.

CONCLUSION

Ordered mesoporous silica type SBA-15 and KIT-6 can be good host matrix for the stabilization of highly dispersed manganese-ceria oxide particles by their predominant location into the mesopores.

The more opened porous structure of KIT-6 facilitates the interaction between the individual oxides. The increase in the ceria content in binary materials results in a decrease in the catalytic activity but preservation of relatively high selectivity to CO_2, and this effect could be successfully controlled by the pore topology of silica support.

Table 2. Data from temperature-programmed reduction

Sample	T_{ini}, K	T_{max}, K	Total weight loss, mg (510–770 K)	Theoretic weight loss, mg	Reduction degree, %
Ce/SBA-15	522	770	0.05	0.14	36
Ce/KIT-6	653	780	0.08		57
2Mn4Ce/SBA-15	535	596	0.18	0.20(0.32)	90(56)
2Mn4Ce/KIT-6	530	597	0.25		125(71)
3Mn3Ce/SBA-15	553	586	0.24	0.25(0.42)	96(26)
3Mn3Ce /KIT-6	560	600	0.14		56(33)
4Mn2Ce/SBA-15	555	580	0.25	0.28(0.51)	89(47)
4Mn2Ce/ KIT-6	540	560	0.16		57(32)
Mn/SBA-15	505	543,610	0.30	0.35(0.70)	86(43)
Mn/KIT-6	517	549,668	0.43		122(61)

T_{ini} - initial reduction temperature, T_{max} - maximum of the reduction peak; reduction degree calculated for Mn^{3+} to Mn^{2+} or Mn^{4+} to Mn^{2+} (in brackets) transition.

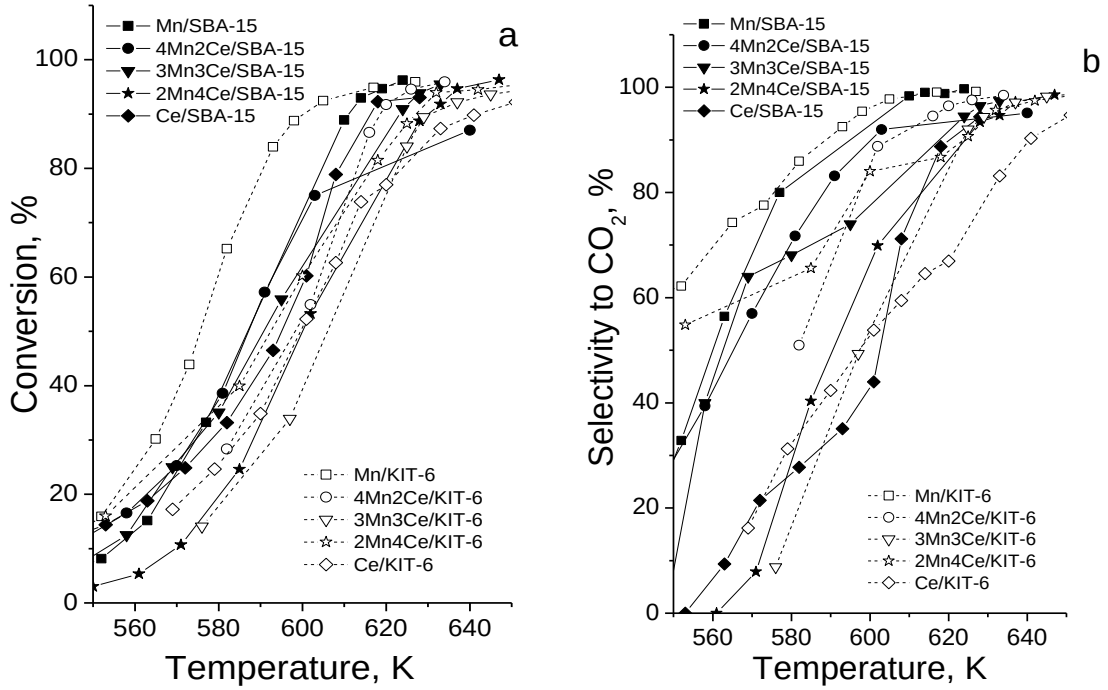

Fig. 5. Catalytic activity (a) and selectivity to CO_2 (b) in ethyl acetate oxidation over SBA-15 and KIT-6 manganese-ceria modifications.

Table 3. Products distribution (wt.%) at 30% conversion for all studied samples.

Sample composition	SBA-15 modifications					KIT-6 modifications				
	Selectivity, %				Conversion at 590 K, %	Selectivity ,%				Conversion at 590 K, %
	AA	Et	AcAc	CO_2		AA	Et	AcAc	CO_2	
CeO_2	23	39	10	28	42	17	32	7	44	34
$2Mn_4Ce$	16	33	10	41	31	11	16	3	70	46
$3Mn_3Ce$	8	14	3	75	48	10	12	2	76	27
$4Mn_2Ce$	11	23	8	58	55	3	11	3	83	38
Mn_xO_y	5	12	3	80	55	3	6	1	90	78

Acknowledgements: *Financial support by Program for career development of young scientists, BAS (project DFNP 145 /12.05.2016) is gratefully acknowledged.*

REFERENCES

1. G. Picasso, R. Cruz, M. del Rosario Sun Kou, *Mater. Res. Bull.*, **70**, 621 (2015).
2. T. Tsoncheva, R. Ivanova, M. Dimitrov, D. Paneva, D. Kovacheva, J. Henych, P. Vomáčka, M. Kormunda, N. Velinov, I. Mitov, V. Štengl, *Appl. Catal. A Gen.*, **528,** 24 (2016).
3. D. Delimaris, T. Ioannides, *Appl. Catal. B: Environ*, **89**, 295 (2009).
4. P. Papaefthimiou, T. Ioannides, X. Verykios, *Appl. Therm. Eng.*, **18**, 1005 (1998).
5. C. Hu, *Chem. Eng. J.*, **168**, 1185 (2011).
6. P. Heynderickx, J. Thybaut, H. Poelman, D. Poelman, G. Marin, *J. Catal.*, **272**, 109 (2010).
7. T. Tsoncheva, G. Issa, T. Blasco, M. Dimitrov, M. Popova, S. Hernández, D. Kovacheva, G. Atanasova, J. M. López Nieto, *Appl. Catal. A Gen.*, **453**, 1 (2013).
8. W. Li, J. Wang, H. Gong, *Catal.Today*, **148**, 81 (2009).
9. S. Todorova, A. Naydenov, H. Kolev, K. Tenchev, G. Ivanov, G. Kadinov, J. *Mater. Sci*., **46**, 7152 (2011).
10. Y. Yang, J. Huang, S. Wang, S. Deng, B. Wang, G. Yu, *Appl. Catal. B Environ.*, **142-143**, 568 (2013).
11. G. Picasso, M. Gutiérrez, M. P. Pina, J. Herguido, *Chem. Eng. J*., **126**, 119 (2007).
12. G. Qi, R. Yang, R. Chang, *Appl. Catal. B Environ*., **51**, 93 (2004).
13. X. Wu, F. Lin, H. Xu, D. Weng, *Appl. Catal. B Environ*., **96**, 101 (2010).
14. M. Choi, W. Heo, F. Kleitz, R. Ryoo, *Chem. Commun.*, 1340 (2003).
15. F. Kleitz, S. H. Choi, R. Ryoo, *Chem. Commun*., 2136 (2003).
16. T. Tsoncheva, G. Issa, J. M. Nieto, T. Blasco, P. Concepcion, M. Dimitrov, G. Atanasova, D. Kovacheva, *Micropor. Mesopor. Mat.*, **180**, 156 (2013).
17. A. Kambolis, H. Matralis, A. Trovarelli, Ch. Papadopoulou, *Appl. Catal. A Gen.*, **377**, 16 (2010).
18. Q. Tang, S. Hu, Y. Chen, Z. Guo, Y. Hub, Y. Chen, Y. Yang, *Micropor. Mesopor. Mater.*, **132**, 501 (2010).
19. Y. Liao, M. Fu, L.Chen, J. Wu, B. Huang, D. Ye, *Catal. Today.*, **216**, 220 (2013).
20. H. Péreza, P. Navarro, J. J. Delgado, M. Montes, *Appl. Catal. A Gen.*, **400**, 238 (2011).
21. P.-O. Larsson, A. Andersson, *Appl. Catal. B Environ.*, **24**, 175 (2000).

ПЪЛНО ОКИСЛЕНИЕ НА ЕТИЛАЦЕТАТ ВЪРХУ НАНОСТРУКТУРИРАНИ МАНГАН-ЦЕРИЕВО ОКСИДНИ КАТАЛИЗАТОРИ НАНЕСЕНИ ВЪРХУ МЕЗОПОРЕСТИ СИЛИКАТИ

Р. Н. Иванова*, Т. С. Цончева

Институт по Органична Химия с Център по Фитохимия, БАН, София, България

Постъпила на 21 февруари 2017 г.; Коригирана на 08 март 2017 г.

(Резюме)

Настоящото изследване е насочено към ефекта от текстурата на мезопорести силикати върху структурните, редокс и каталитични свойства на нанесени наноразмерни моно- и би-компонентни манган-цериеви оксиди. Мезопорести силикати тип SBA-15 и KIT-6 с еднакви цилиндрични мезопори подредени в 2D- и 3D- симетрия, бяха използвани като носители. Комплекс от физикохимични техники, като азотна физисорбция, прахова рентгенова дифракция, UV-Vis спектроскопия и температурно-програмирана редукция с водород бяха използвани за характеризиране на образците. Беше изследвано потенциалното приложение на композитите като катализатори за окисление на етилацетат. Беше демонстрирано, че SBA-15 и KIT-6 могат да бъдат добра матрица за стабилизирането на високо дисперсни манган-цериево оксидни частици. Беше установен силен ефект от топологията на мезопорестия носител, който също зависи и от състава на образците, върху формирането на каталитично активните фази.